Dynamic Thermal Effect in a Hollow Core Microbottle Resonator

Zhe Wang, Zhuochen Wang, Anuradha Rout, Rayhan Habib Jibon, Anand V. R, Fangfang Wei, Qiang Wu, and Yuliya Semenova

***Abstract*—Dynamic thermal wavelength shift in hollow core microbottle resonators has been experimentally demonstrated using the frequency-detuning method. A linewidth broadening phenomenon is observed when the tunable laser is swept from a shorter wavelength to a longer wavelength. The thermal effect in the microbottles with various diameters as a function of the power and sweep frequency of the tunable laser has been studied and analyzed. In addition, the effect of thermal broadening on multiple WGM resonances within the spectrum has been observed, demonstrating that broadening of the linewidth of the first WGM resonance suppresses the subsequent WGM resonances during the up-scanning cycle of the tunable laser. Study of the dynamic response of the microbottle is beneficial for the design of ultrahigh-resolution optical fiber thermometers and low threshold mode-locked lasers.**

***Index Terms*—Dynamic thermal effect, hollow core microbottle, thermo-optic effect, whispering gallery modes.**

I. Introduction

WHISPERING gallery modes (WGMs) have been investigated in recent years for their applications in nonlinear optics [1], microcavity lasers [2], optical signal processing [3], and optical sensing [4] due to the advantages of high quality (Q) factors and small mode volumes. In sensing applications, high Q factors lead to high measurement resolution, making it suitable for low-dose molecules detection in addition to the promising sensing techniques, such as surface plasmon resonance sensors [5], [6], [7], [8], fluorescence sensors [9], [10], [11] and fiber interferometric sensors [12], [13], [14]. Alongside this, the high Q factor facilities the study of the nonlinear phenomena in microcavities such as electromagnetically induced transparency [15], Kerr frequency combs [16] and thermo-optic dynamics [17]. When light with a specific wavelength is trapped in a microcavity, a small portion of it is absorbed by the cavity and converted into heat, which results in changes of the refractive index and the diameter of the microresonator, leading to a spectral shift of the WGM resonant wavelength. Since the heat is dissipated from the microcavity through its surface area, thermal effects that are usually negligible in large cavities, can be significant.

A study of the dynamic thermal behavior of a toroidal microcavity was reported by Carmon et al. in [18] who analyzed the thermally induced hysteretic wavelength response of the cavity and derived a dynamical formula describing the behavior. The authors demonstrated that regardless of the direction of the tunable pump laser scan (from short to long wavelengths or vice versa), the WGM resonance always drifted towards the longer wavelength. However, when the pump wavelength scan direction was towards longer wavelengths, a greater amount of pump power was coupled into the resonator. As a result, an asymmetric line broadening and hysteretic wavelength response phenomena were observed. Based on the studies of a silica microcavity, the dynamic thermal behavior of a polydimethylsiloxane (PDMS) coated silica toroidal microcavity was investigated, where the opposite thermo-optic effects in silica cavity and PDMS coating led to oscillatory thermal dynamics [19]. Furthermore, a method aimed at estimating the thermal relaxation of a microdisk was also illustrated by fitting two adjacent WGM resonances that were tuned by thermal effects [20].

Studies of the dynamic thermal behavior of microresonant cavities are useful for a better understanding of heat accumulation and dissipation processes, which can be exploited for the development of high-sensitivity sensors and mode-locked lasers. In sensing applications, any thermally induced shift is highly undesirable as it can influence the total spectral resonance shift induced by the refractive index change. Therefore, a thermally induced shift should be calibrated to ensure the accuracy of the sensor. Alternatively, several thermal stabilization techniques have been developed to suppress the thermal effects in microcavities. For example, a thermometer with less than milli-Kelvin self-heating effect composed of a silicon nitride (Si_3N_4) microring was proposed and experimentally demonstrated in [21]. On the other hand, the heat energy accumulation due to the thermal phenomena can be used to design self-locking lasers. For example, Lin et al. demonstrated frequency locking in Raman optical frequency combs using a BaF_2 disk resonator with an ultrahigh Q-factor [22].

Manuscript received 15 March 2024; revised 3 June 2024; accepted 11 June 2024. Date of publication 21 June 2024; date of current version 16 September 2024. This work was supported in part by Science Foundation Ireland under Grant 13/RC/2077_P2 and Grant 18/CRT/6222, in part by Fiosraigh Scholarship Award 2019 (TU Dublin), and in part by Royal Society International Exchanges 2022 under Grant IES\R3\223005. *(Corresponding author: Zhe Wang.)*

Zhe Wang, Zhuochen Wang, Anuradha Rout, Rayhan Habib Jibon, Anand V. R, Fangfang Wei, and Yuliya Semenova are with the Photonics Research Centre, School of Electrical and Electronic Engineering, Technological University Dublin, D07 ADY7 Dublin 7, Ireland (e-mail: d19125415@mytudublin.ie; d18130040@mytudublin.ie; d19125690@mytudublin.ie; d22124683@mytudublin.ie; anand.vr@tudublin.ie; fangfang.wei@tudublin.ie; yuliya.semenova@tudublin.ie).

Qiang Wu is with the Department of Mathematics, Physics and Electrical Engineering, Northumbria University, NE1 8ST Newcastle Upon Tyne, U.K. (e-mail: qiang.wu@northumbria.ac.uk).

Color versions of one or more figures in this article are available at https://doi.org/10.1109/JLT.2024.3417712.

Digital Object Identifier 10.1109/JLT.2024.3417712

As one of the geometries that supports the WGMs, microbottles offer the advantages of higher Q factors and improved coupling stability compared with other WGM structures [23], [24], facilitating their applications in sensing and microlasers with high sensitivity and good stability. The hollow-core structure allows for filling the microresonator with various materials with special properties, enabling the control of modes by changing the effective refractive index and diameter of the microcavity [25]. The flexibility in mode selection maintains the robustness of coupling states, making it an ideal platform for various applications based on the thermo-optic effect within the microbottle compared with other WGMs structures. Though the dynamic thermal effects in microcavities with various geometries and materials have been investigated previously, our study of the dynamic thermal effect in a hollow core microbottle lays the foundation for enhancing materials-filled microbottle sensors' sensitivities by decreasing the thermal induced errors and improving microbottle lasers' efficiency by decreasing the lasing threshold. In addition, it will be beneficial to researchers focusing on the nonlinear optical effects based on the hollow-core microbottles, paving the way for more applications of WGMs, such as wavelength-division multiplexed coherent communications [26], Brillouin lasers [27], and Raman spectroscopy [28].

In this work, we for the first time experimentally demonstrate and analyze thermal effects in hollow core silica microbottles with Q factors in the order of 10^7 using the frequency-detuning method. The differences in the wavelength response for hollow core microbottles have been investigated as a function of the power and sweeping frequency of the pump laser. The heat accumulation induced wavelength shift during the laser scanning has been investigated. Furthermore, the wavelength response of multiple WGM resonances have been studied, demonstrating the effect of heat accumulation and distribution among multiple WGM resonances. The lineshapes of the WGM resonances in the transmission spectra during the upward scanning cycle of the tunable laser were also studied experimentally. To the best of our knowledge, this is the first report focusing on dynamic thermal effects of multiple WGM resonances, which is beneficial for expanding their applications in sensing, microlasers and spectroscopy.

II. Experimental Setup and Sample Preparation

The hollow core microbottles were fabricated by tapering thick-wall silica capillaries using a customized microheater brushing technique [29]. In each case a central section (approximately 5 cm long) of the capillary with outer and inner diameters of 450 μm and 300 μm (Polymicro Technology), was stripped off and placed inside the microheater slit where the temperature was set to 1300 °C. The temperature of the microheater was optimized to ensure the viscoelastic state of the silica fiber or capillary, making it suitable for the tapering process. Opposite ends of the capillary were fixed on the translation stages whose motion was accurately controlled by a custom-built computer program. The tapering process lasted for 15 mins, resulting in

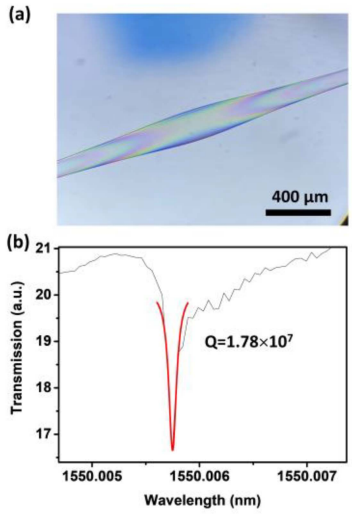

Fig. 1. (a) Microscopic image of the hollow-core microbottle, (b) transmission spectrum of the fiber taper coupled to the hollow-core microbottle and the Lorentzian fit of the resonance at 1550.0057 nm.

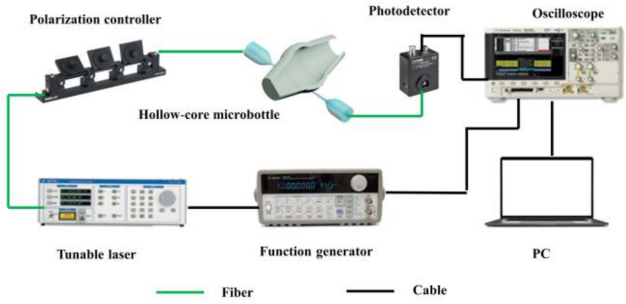

Fig. 2. Schematic diagram of the experimental setup.

fabrication of a tapered capillary with an outer diameter of 35 μm and wall thickness of 2.5 μm.

To fabricate a hollow microbottle, one end of the tapered capillary was sealed using a UV-curable glue whereas the other end was connected to a syringe pump that provided air pressure. The tapered capillary was then kept inside the slit for further 5 mins before injecting the air with the syringe. This resulted in the fabrication of a hollow core microbottle with a maximum outer diameter of 177 μm as shown in Fig. 1(a). The microbottle was then disconnected from the syringe pump and fixed on a glass slide using two drops of a UV-curable glue.

A tapered fiber with a waist diameter of 2 μm was fabricated by heating and stretching a commercial single mode fiber (SMF) with a diameter of 125 μm using the same microheater brushing setup. The experimental setup for characterization of the microbottle is illustrated in Fig. 2. Two ends of the fabricated tapered fiber were connected to the tunable laser (Anritsu, Tunics Plus) through a polarization controller (Thorlabs, FPC561), a photodetector (Thorlabs, PDA10CS-EC) and an oscilloscope (Keysight MSO-X 2022A), respectively. The polarization controller was utilized to optimize the transmission spectrum with high Q-factor WGM resonances. The paddles of polarization

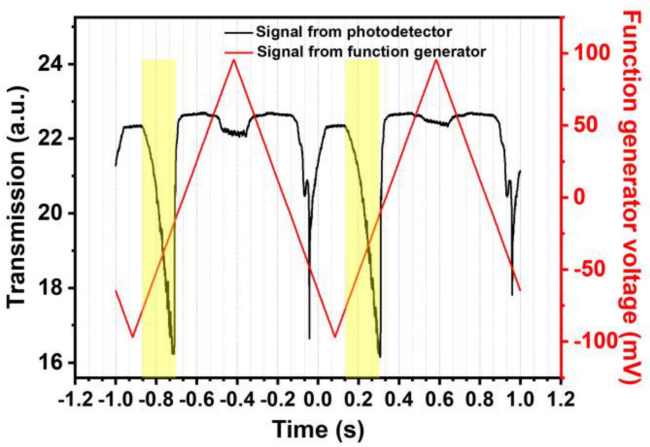

Fig. 3. Dynamic response of the hollow core microbottle at 4 mW pump laser power (black) and function generator signal (red).

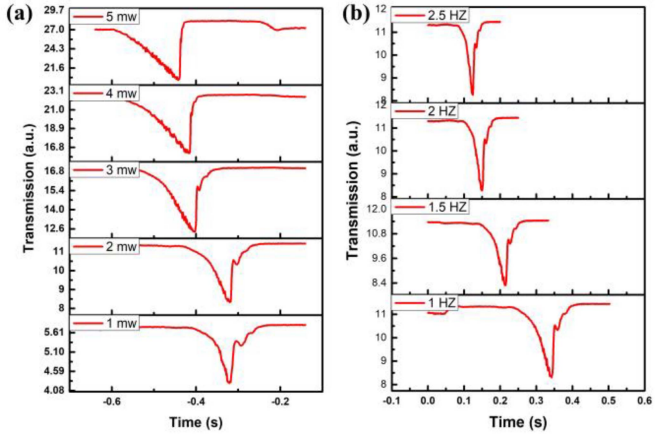

Fig. 4. Dynamic transmission responses of the hollow core microbottle at (a) different pump powers and constant scanning frequency of 1 Hz, (b) different laser scanning frequencies and fixed pump laser power of 2 mW.

controller were fixed once the transmission spectrum with high Q-factor resonance dips was obtained ensuring the consistency of the experiments. A function generator (Agilent, 33120A) was used to control the wavelength scanning frequency of the tunable laser. The glass slide with the microbottle was placed on a 3-dimensional translation stage perpendicularly close to the tapered fiber to facilitate the most efficient light coupling. To estimate the Q-factor of the hollow-core microbottle, the time-domain signal from the photodetector is converted to the wavelength-domain spectrum according to the central wavelength of the tunable laser and the voltage from the function generator. The experiments were conducted in a laboratory with an ambient temperature of 18±0.5 °C. It should be noted the minor temperature changes occurred in a slow manner and did not substantially influence the linewidth broadening effect within a time range of 500 ms in the subsequent experiments. The transmission spectrum of the fiber taper coupled to the hollow core microbottle is shown in Fig. 1(b). The Q-factor for the resonance near 1550.0057 nm was estimated as 1.78×10^7 and the full width at half maximum (FWHM) as 2 pm using a Lorentzian fit.

III. Experimental Results and Discussion

A. Dynamics of a Single WGM Resonance

The dynamic response of the hollow core microbottle (with a 140.5 μm diameter) recorded with the scanning frequency of 1 Hz and pump laser power of 4 mW is shown in Fig. 3. The low-to-high parts of the function generator signal (red line) correspond to the pump wavelength sweep in the direction from short to long wavelengths, and vice versa. As can be seen from the graph, when the scanning wavelength approaches the cavity resonance from the shorter wavelength side, light is trapped inside the microcavity where the thermal effect leads to a small change of the cavity diameter and the refractive index, leading to a red shift of the resonance wavelength. Since the direction of the wavelength scanning and the wavelength shift of the resonance coincide, further energy accumulation within the microbottle leads to a broader linewidth as shown in Fig. 3 during −0.9–0.7 s (highlighted in yellow). On the other side of the dip, beyond −0.7 s point, the resonant wavelength does not red-shift any further because the heat accumulation cannot compensate for the heat dissipation from the cavity. Similar linewidth broadening is observed during the time interval 0.1–0.3 s (highlighted in yellow) in the second up-scanning sweep. In the case of the wavelength down-scanning process, a narrowed resonance is observed due to opposite directions the tunable laser scanning (blue shift) and the resonance wavelength shift (red shift). The coupling efficiency can be calculated as 28.3% based on the transmission decrease near the resonant dip in Fig. 3 [30].

Plots in Fig. 4 demonstrate the dynamic responses of the hollow-core microbottle (177 μm) at various pump laser powers and a fixed scanning frequency of 1 Hz (a), and various scanning frequencies and laser power fixed at 2 mW during the up-scanning cycle (b). As can be seen from the plots, a larger hysteretic dynamic effect is observed at higher pump laser powers. In contrast, a smaller hysteric effect is observed when the pump signal is swept with a higher frequency. This can be explained by the limited speed of the thermal response of the cavity to the fast-scanning pump signal. To demonstrate the wavelength shift arising from the thermal hysteric effect, the time dependency was converted to the wavelength dependency during the up-scanning cycle according to the central wavelength and the voltage signal applied to the tunable laser. Fig. 5(a) and (b) illustrate the resonance shift as a function of the pump power and scanning frequency of the tunable laser for the hollow core microbottles with outer diameters of 98.9 μm (wall thickness of 1.9 μm), 140.5 μm (wall thickness of 1.6 μm), and 177 μm (wall thickness of 1.5 μm), respectively. As one can see, larger resonance wavelength shifts occur at higher pump powers and smaller scanning frequencies of the tunable laser for three hollow core microbottle samples. The increase of the input laser power leads to higher energy accumulation inside the

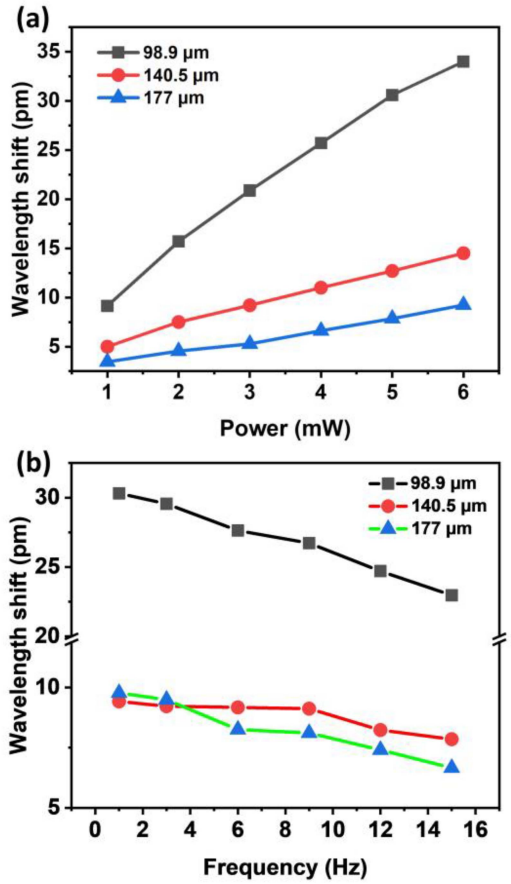

Fig. 5. Wavelength shift for the selected spectral dip versus (a) pump power (b) scanning frequency for hollow-core microbottles with diameters of 98.9 μm, 140.5 μm, and 177 μm.

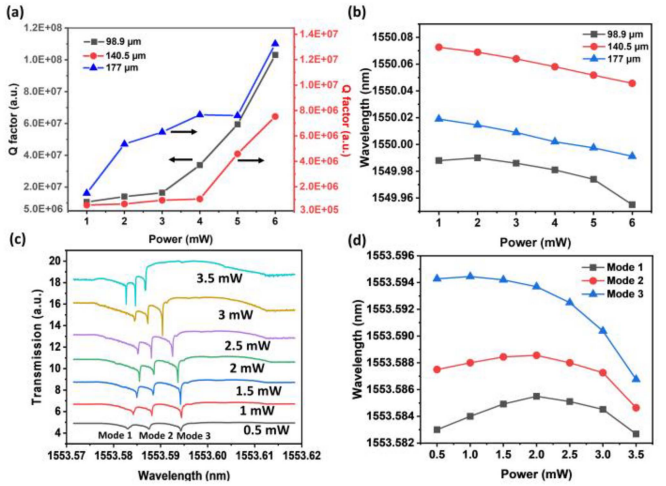

Fig. 6. (a) Q factor and (b) wavelength of the WGM resonance at various laser powers for microbottles with diameters of 98.9, 140.5 and 177 μm, (c) experimental transmission spectra of a hollow core microbottle at various tunable laser powers, (d) wavelengths of the WGM resonant dips versus the power of the scanning tunable laser.

microbottle due to the absorption within the silica, contributing to a broader linewidth demonstrated in Fig. 4(a). The increase in the scanning frequency leads to a weaker linewidth broadening effect which can be attributed to a lower amount of energy accumulation in the hollow-core microbottle. Since the speed with which the heat energy is absorbed and dissipated by the resonator resulting in the change of its diameter and subsequent spectral shift of the WGM wavelength is limited, the increase in the scanning frequency leads to a narrower linewidth of the resonance.

To investigate the dependency of the linewidth broadening effect of the wavelength resonance versus the power of the tunable laser, the spectra of the down-scanning cycles were recorded for hollow core microbottles with various diameters whose corresponding Q factors are illustrated in Fig. 6(a). It can be seen that the Q factor of the wavelength resonance increases with the increase of the input power for all the microbottles, indicating lower energy dissipation with respect to absorption. The lower heat dissipation by the microbottle at higher tunable laser powers contributes to the heat accumulation when shifting to a longer wavelength, which explains the stronger broadening effect observed in the WGM spectra during the upward scanning cycle, as depicted in Fig. 5(a). Fig. 6(a) also demonstrates that the resonance broadening effect caused by the thermal effect is positively related to the Q factor, where a larger linewidth broadening effect usually happens for the resonator mode with a higher Q factor. Fig. 6(b) illustrates the dependency of the spectral position of the WGM resonance with respect to the power of the tunable laser for 3 microbottles with different diameters during the downward scanning cycle. As can be seen from the figure, the WGM resonance shifts towards shorter wavelengths with an increase of the laser power for microbottles with diameters of 140.5 μm and 177 μm. This observed blue shift could be attributed to the displacement and structural deformation of the hollow core microbottle under the influence of optical field induced in the coupling taper by the tunable laser at higher powers [31], [32]. It can also be observed that the WGM resonance for the 98.9-μm microbottle undergoes a redshift within the power range of 1–2 mW, subsequently experiencing a blueshift with a further increase of the input laser power. The red shift of the resonance is ascribed to the increase in the diameter of the hollow microbottle induced by the radiation pressure exerted by the light coupled through the tapered fiber [33]. To illustrate the wavelength shift tendency of the 98.9-μm microbottle in a power range of 0.5–3.5 mW, various laser powers were pumped into the WGM coupling system with an interval of 0.5 mW and the corresponding transmission spectra are shown in Fig. 6(c). As one can see, the wavelength spectrum initially exhibits a red shift with increasing laser power, whereas continued increments in the pump power lead to a subsequent blue shift. Fig. 6(d) demonstrates the dependency of the wavelength resonances for three different modes versus the tunable laser power. It can be seen that all WGM resonance modes experience a redshift and a subsequent blueshift as the increase of the laser power, though exhibiting different turning points. Initially, the effect of thermal expansion of the hollow core microbottle dominates resulting in the red shift, whereas at higher power levels effects caused by the optical forces induced by the fiber taper begin to dominate, leading to blue shifts of the WGM resonances.

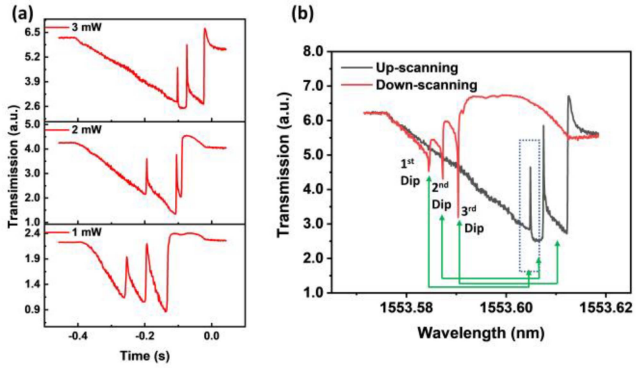

Fig. 7. (a) Dynamic response of the hollow core microbottle with a diameter of 98.9 μm at different laser powers, (b) wavelength response of the hollow core microbottle with 3 mW input laser power.

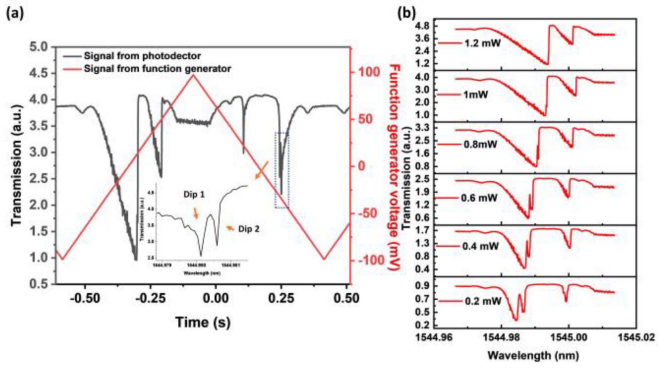

Fig. 8. (a) Dynamic response of the hollow core microbottle (98.9 μm) at 1.2 mW pump laser power (black) and function generator signal (red), (b) transmission spectra of the hollow core microbottle at different pump laser power.

B. Dynamics of Multiple WGM Resonances

The WGM spectra of a hollow core microbottle (98.9 μm) with multiple WGM resonance dips recorded at the scanning frequency of 1 Hz and various pump laser powers are shown in Fig. 7(a). As one can see from the graph, due to the spectral proximity of multiple resonances, the linewidth broadening phenomenon observed in the previous experiments for the shortest wavelength resonance leads to the suppression of the linewidths of subsequent resonance dips during the up-scanning cycle, and this suppression becomes more pronounces with the increase in the tunable laser power. The second WGM resonance also has a suppressive effect with respect to the third (longest wavelength) resonance. The transmission of the hollow-core microbottle with 1-Hz scanning frequency and input pump laser of 3 mW is shown in Fig. 7(b). It can be observed that the first (shortest) resonance of the microbottle shifts and closely tracks the wavelength of the tunable laser. Similar to the case of a single WGM resonance, the absorption leads to the change of the cavity's diameter and refractive index, resulting in a continuing thermal accumulation and the linewidth broadening effect due to the match between the resonant wavelength and the wavelength of the tunable laser. Then the first resonance does not red-shift any further when the tunable laser up-scans around 1553.6025 nm, where the heat accumulation cannot compensate for the heat dissipation from the cavity, leading to a sharp transmission increase in the spectrum as shown in the dashed box in Fig. 7(b). This heat dissipation process lasts for 0.1 ms according to the frequency-detuning spectra demonstrated in Fig. 7(a), which can be attributed to the thermal mechanism involving the heat dissipation from the mode volume to the rest of the hollow core bottle, where the relaxation time is in the order of milliseconds. Heat transfer between the hollow-core microbottle and the surroundings over the period of tens of milliseconds is not considered [19]. The temperature change when the heat accumulation cannot counteract the heat dissipation can be described by the equation: $\Delta T\,(t) = T_0\, e^{(-t-t_0)/\tau}$, where T_0 is the maximum temperature change of the microcavity, t_0 is the corresponding time during which this change has occurred, t is the time variable, and τ is the thermal relaxation time [34]. The temperature of the microcavity decreases exponentially until it reaches the initial microcavity temperature where the ΔT is 0. Then, since the wavelength shift caused by the change of the cavity's diameter and refractive index is also applicable to the second resonance, the consistency between the second resonance and the wavelength of the scanning laser leads to a significant transmission decrease, where the remaining heat energy within the microbottle contributes to the linewidth broadening of the second WGM resonance. Similarly, the emergence of the third WGM resonant mode can also lead to a notable transmission reduction and a sharp edge in the transmission spectrum. The linewidth broadening will disappear when the heat accumulation cannot counteract the exponential thermal decay. It should be noted the different resonant modes show different sensitivities with respect to the diameter and refractive index changes of the microcavity due to the thermal absorption, in accordance with the plot in Fig. 6(d), where smaller wavelength gaps between WGM resonances with the increase in the pump laser power led to wavelength mismatch between the resonances and the scanning laser. Thus, the heat accumulation tends to be lower than heat dissipation in terms of multiple WGM resonances in a microcavity, demonstrating suppressions of the linewidth broadening for the second and third WGM resonances.

To further investigate the linewidth broadening of the multiple WGM resonance modes, two adjacent WGM resonance dips in the transmission spectrum were studied. Fig. 8(a) shows the dynamic response of the microbottle (98.9 μm) at the tunable laser power of 1.2 mW. As depicted in the inset spectrum in Fig. 8(a), Dip 1 has central wavelength at 1544.98014 nm and Dip 2 - at 1544.98059 nm. It should be noted the horizontal coordinate of the inset is converted to the wavelength units to better illustrate the spectral gap of 0.45 pm between the two dips. Fig. 8(b) shows the transmission spectra of the microbottle (98.9 μm) at different laser powers, where the linewidth broadening effect of the first dip can be clearly observed. It can also be seen that the increase in the tunable laser power leads to a larger linewidth broadening of Dip 1 and a complete suppression of Dip 2 at higher powers. This is attributed to the wavelength mismatch between the WGM resonances and the up-scanning laser caused by changes in the

TABLE I
COMPARISON OF THERMAL-OPTIC DYNAMIC EFFECT FOR DIFFERENT TYPES OF MICRORESONATORS

Geometry	Material	Diameter (μm)	Laser power (mW)	Scanning speed or frequency	Wavelength shift (pm)	Reference
Sphere	Silica	140	1	4.6 nm/s	60	[18]
Sphere	Silica	25	1	50 Hz	70	[37]
PDMS coated toroid	PDMS and silica	42.2	3.1	40 nm/s	3	[19]
Ring	Si_3N_4	200	2.10	0.05 nm/s	30	[21]
Disk	Silicon	4.5	0.035	4 MHz	200	[36]
Hollow core bottle	Silica	144	2	1 Hz	16	Our work

diameter and refractive index of the microcavity. As the laser power increases, the second WGM resonance cannot follow the up-scanning laser, demonstrating the suppression of Dip 2. A complete wavelength match with the increase in the laser power results in a complete suppression of Dip 2.

C. Comparison of Different WGM Microresonators

A comparison of the thermo-optic dynamic effect for different types of WGM microresonators reported in literature to date with the results of this work has been carried out. As can be seen from Table I, the linewidth broadening effect can be observed in all types of WGM geometries for lasers operating in the power range of milliwatts. Due to the larger thermo-optic coefficient of silicon ($\sim 10^{-4}$ K^{-1}) [35], a stronger linewidth broadening was achieved for a microdisk with a diameter of 4.5 μm despite a smaller operating laser power and a higher scanning frequency [36]. Based on the study of the silica microsphere in [18], the linewidth broadening effect with respect to the laser power and scanning frequency have been investigated in [37], demonstrating a larger wavelength shift compared with our result. The linewidth broadening effect can be mitigated by coating the resonator with a layer of PDMS, where the negative thermo-optic coefficient of PDMS compensates for the wavelength shift caused by the diameter expansion of the silica resonator [19]. Due to the hollow core feature in our case, thermal expansion of silica occurs only in the microbottle walls, leading to a smaller wavelength shift similar to the result reported for a Si_3N_4 ring [21]. The observation can be applied to sensors with high sensitivities, lasers with low thresholds, and nonlinear optics with reduced thermal noise.

IV. CONCLUSION

In conclusion, the dynamics of the thermo-optic effect in hollow core microbottle resonators with Q factors in the order of 10^7 have been investigated using the frequency-detuning method. By sweeping the tunable laser towards longer or shorter wavelengths with the help of a signal generator, we observed the differences in the spectral shifts of WGM resonances and the resonance broadening due to the differences in light absorption and heat dissipation mechanisms within the cavity. Owing to the heat dissipation by the microresonator cavity being a slower process than light absorption over a short sweep period, the hysteretic response has been detected using an oscilloscope in a high-resolution mode. The differences in the resonators' response were also studied as a function of the power and sweeping frequency of the pump laser. The results indicate that a higher tunable laser power and a lower scanning frequency both lead to a larger wavelength shift during the up-scanning process. The dependency of the WGM resonant wavelengths with respect to the power of tunable laser was investigated at various laser powers. The spectral dynamics of multiple WGM resonances were studied with respect to the power of the tunable laser. The continued linewidth broadening in multiple WGM resonances shows the heat accumulation in hollow-core resonator, potentially facilitating its applications in sensors and mode-locked lasers.

Conflict of Interest: The authors declare no conflicts of interest regarding this article.

REFERENCES

[1] A. E. Fomin, M. L. Gorodetsky, and V. S. Ilchenko, "Nonstationary nonlinear effects in optical microspheres," *J. Opt. Soc. Amer. B*, vol. 22, no. 2, pp. 459–465, 2005, doi: 10.1364/JOSAB.22.000459.

[2] M. Mur et al., "Magnetic-field tuning of whispering gallery mode lasing from ferromagnetic nematic liquid crystal microdroplets," *Opt. Exp.*, vol. 25, no. 2, pp. 1073–1083, Jan. 2017, doi: 10.1364/oe.25.001073.

[3] F. Monifi, Ş. K. Özdemir, and L. Yang, "Tunable add-drop filter using an active whispering gallery mode microcavity," *Appl. Phys. Lett.*, vol. 103, no. 18, Oct. 2013, doi: 10.1063/1.4827637.

[4] A. Mahmood, V. Kavungal, S. S. Ahmed, G. Farrell, and Y. Semenova, "Magnetic-field sensor based on whispering-gallery modes in a photonic crystal fiber infiltrated with magnetic fluid," *Opt. Lett.*, vol. 40, no. 21, pp. 4983–4985, 2016, doi: 10.1364/OL.40.004983.

[5] Z. Chen et al., "Ultrasensitive DNA origami plasmon sensor for accurate detection in circulating tumor DNAs," *Laser Photon Rev.*, 2024, doi: 10.1002/lpor.202400035.

[6] T. Xue et al., "Ultrasensitive detection of miRNA with an antimonene-based surface plasmon resonance sensor," *Nature Commun.*, vol. 10, no. 1, Dec. 2019, Art. no. 28, doi: 10.1038/s41467-018-07947-8.

[7] F. Zheng et al., "A highly sensitive CRISPR-empowered surface plasmon resonance sensor for diagnosis of inherited diseases with femtomolar-level real-time quantification," *Adv. Sci.*, vol. 9, no. 14, May 2022, Art. no. 2105231, doi: 10.1002/advs.202105231.

[8] Z. Chen et al., "A CRISPR/Cas12a-empowered surface plasmon resonance platform for rapid and specific diagnosis of the Omicron variant of SARS-CoV-2," *Nat. Sci. Rev.*, vol. 9, no. 8, Aug. 2022, Art. no. nwac104, doi: 10.1093/nsr/nwac104.

[9] Y. H. Shin, J. Z. Barnett, M. T. Gutierrez-Wing, K. A. Rusch, and J. W. Choi, "A hand-held fluorescent sensor platform for selectively estimating green algae and cyanobacteria biomass," *Sensors Actuators B Chem.*, vol. 262, pp. 938–946, Jun. 2018, doi: 10.1016/j.snb.2018.02.045.

[10] F. Katzmeier et al., "A low-cost fluorescence reader for in vitro transcription and nucleic acid detection with Cas13a," *PLoS One*, vol. 14, no. 12, Dec. 2019, Art. no. e0220091, doi: 10.1371/journal.pone.0220091.

[11] T. Skorjanc, D. Shetty, and M. Valant, "Covalent organic polymers and frameworks for fluorescence-based sensors," *ACS Sensors*, vol. 6, no. 4, pp. 1461–1481, Apr. 2021, doi: 10.1021/acssensors.1c00183.

[12] J. Amorebieta et al., "Compact omnidirectional multicore fiber-based vector bending sensor," *Sci. Rep.*, vol. 11, no. 1, Dec. 2021, Art. no. 5989, doi: 10.1038/s41598-021-85507-9.

[13] J. Villatoro, "Phase-shifted modal interferometers for high-accuracy optical fiber sensing," *Opt. Lett.*, vol. 45, no. 1, pp. 21–24, Jan. 2020, doi: 10.1364/ol.45.000021.

[14] Y. Ouyang et al., "An in-fiber dual air-cavity Fabry–Perot interferometer for simultaneous measurement of strain and directional bend," *IEEE Sensors J.*, vol. 17, no. 11, pp. 3362–3366, Jun. 2017, doi: 10.1109/JSEN.2017.2693501.

[15] X. Jin, Y. Dong, and K. Wang, "Stable controlling of electromagnetically induced transparency-like in a single quasi-cylindrical microresonator," *Opt. Exp.*, vol. 24, no. 26, pp. 29773–29780, Dec. 2016, doi: 10.1364/oe.24.029773.

[16] S. Zhu et al., "Controllable Kerr and Raman-Kerr frequency combs in functionalized microsphere resonators," *Nanophotonics*, vol. 8, pp. 2321–2329, 2019, doi: 10.1515/nanoph-2019-0342.

[17] X. Jiang and L. Yang, "Optothermal dynamics in whispering-gallery microresonators," *Light: Sci. Appl.*, vol. 9, no. 1, Dec. 2020, Art. no. 24, doi: 10.1038/s41377-019-0239-6.

[18] T. Carmon, L. Yang, and K. J. Vahala, "Dynamical thermal behavior and thermal self-stability of microcavities," *Opt. Exp.*, vol. 12, no. 20, pp. 4742–4750, 2004, doi: 10.1364/OPEX.12.004742.

[19] L. He, Y.-F. Xiao, J. Zhu, S. K. Ozdemir, and L. Yang, "Oscillatory thermal dynamics in high-Q PDMS-coated silica toroidal microresonators," *Opt. Exp.*, vol. 137, no. 8, pp. 9571–9581, 2009, doi: 10.1364/OE.17.009571.

[20] W. Chen, J. Zhu, Ş. K. Özdemir, B. Peng, and L. Yang, "A simple method for characterizing and engineering thermal relaxation of an optical microcavity," *Appl. Phys. Lett.*, vol. 109, no. 6, Aug. 2016, Art. no. 061103, doi: 10.1063/1.4960665.

[21] C. Zhang et al., "Photonic thermometer by silicon nitride microring resonator with milli-kelvin self-heating effect," *Measurement*, vol. 188, Jan. 2022, Art. no. 110494, doi: 10.1016/j.measurement.2021.110494.

[22] G. Lin and Y. K. Chembo, "Phase-locking transition in Raman combs generated with whispering gallery mode resonators," *Opt. Lett.*, vol. 41, no. 16, Aug. 2016, Art. no. 3718, doi: 10.1364/ol.41.003718.

[23] M. Sumetsky, "Optical bottle microresonators," *Prog. Quantum Electron.*, vol. 64, pp. 1–30, Mar. 2019, doi: 10.1016/j.pquantelec.2019.04.001.

[24] Y. Louyer, D. Meschede, and A. Rauschenbeutel, "Tunable whispering-gallery-mode resonators for cavity quantum electrodynamics," *Phys. Rev. A*, vol. 72, no. 3, Sep. 2005, Art. no. 031801, doi: 10.1103/PhysRevA.72.031801.

[25] X.-C. Yu et al., "Single-molecule optofluidic microsensor with interface whispering gallery modes," *Proc. Nat. Acad. Sci.*, vol. 119, no. 6, Feb. 2022, Art. no. e2108678119, doi: 10.1073/pnas.2108678119.

[26] J. Pfeifle et al., "Coherent terabit communications with microresonator kerr frequency combs," *Nature Photon.*, vol. 8, no. 5, pp. 375–380, 2014, doi: 10.1038/nphoton.2014.57.

[27] M. Asano et al., "Stimulated Brillouin scattering and Brillouin-coupled four-wave-mixing in a silica microbottle resonator," *Opt. Exp.*, vol. 24, no. 11, pp. 12082–12092, May 2016, doi: 10.1364/oe.24.012082.

[28] W. Mao, Y. Li, X. Jiang, Z. Liu, and L. Yang, "A whispering-gallery scanning microprobe for Raman spectroscopy and imaging," *Light Sci. Appl.*, vol. 12, no. 1, Dec. 2023, Art. no. 247, doi: 10.1038/s41377-023-01276-2.

[29] Z. Wang et al., "Thermo-optic tuning of a nematic liquid crystal-filled capillary whispering gallery mode resonator," *Opt. Exp.*, vol. 29, no. 15, Jul. 2021, Art. no. 23569, doi: 10.1364/oe.432103.

[30] A. E. Shitikov, I. A. Bilenko, N. M. Kondratiev, V. E. Lobanov, A. Markosyan, and M. L. Gorodetsky, "Billion Q-factor in silicon WGM resonators," *Optica*, vol. 5, no. 12, pp. 1525–1528, Dec. 2018, doi: 10.1364/optica.5.001525.

[31] Y. Zhang et al., "Optical fiber tweezers: From fabrication to applications," *Opt. Laser Technol.*, vol. 175, Aug. 2024, Art. no. 110681, doi: 10.1016/j.optlastec.2024.110681.

[32] Y. Wu, J. Ward, and S. Nic Chormaic, "Observation of thermal feedback on the optical coupling noise of a microsphere attached to a low-spring-constant cantilever," *Phys. Rev. A*, vol. 85, no. 5, May 2012, Art. no. 053820, doi: 10.1103/PhysRevA.85.053820.

[33] Y. Liu et al., "Ultrahigh-resolution optical Fiber thermometer based on microcavity opto-mechanical oscillation," *Adv. Photon. Res.*, vol. 3, no. 9, Sep. 2022, Art. no. 2200052, doi: 10.1002/adpr.202200052.

[34] T. Wang, X. F. Liu, Y. Hu, G. Qin, D. Ruan, and G. L. Long, "Rapid and high precision measurement of opto-thermal relaxation with pump-probe method," *Sci. Bull.*, vol. 63, no. 5, pp. 287–292, Mar. 2018, doi: 10.1016/j.scib.2018.02.005.

[35] J. Komma, C. Schwarz, G. Hofmann, D. Heinert, and R. Nawrodt, "Thermo-optic coefficient of silicon at 1550 nm and cryogenic temperatures," *Appl. Phys. Lett.*, vol. 101, no. 4, Jul. 2012, Art. no. 041905, doi: 10.1063/1.4738989.

[36] T. J. Johnson, M. Borselli, and O. Painter, "Self-induced optical modulation of the transmission through a high-Q silicon microdisk resonator," *Opt. Exp.*, vol. 14, no. 2, pp. 817–831, 2006. [Online]. Available: http://www.opticsexpress.org/abstract.cfm?URI=OPEX-13-23-9623

[37] H. Zhou et al., "Real-time observation of the thermo-optical and heat dissipation processes in microsphere resonators," *Opt. Exp.*, vol. 29, no. 2, pp. 2402–2410, Jan. 2021, doi: 10.1364/oe.408568.